Reply to the comments of RC3

RC3: General comment

General comment 1: The revised manuscript is an improvement over the previous version. However, major issues still persist. Specifically, the objectives of the manuscript remain unclear, and the overall structure appears disjointed.

Response: We thank the reviewer for the comment. We apologize if our previous statement wasn't clear enough to re-join the two objectives. Based on the literature review, the dry deposition scheme by Shu et al. (2022) has reduced certain model biases, but the effect of the scheme on the East Asian Dust has not been conducted, which means the dry deposition scheme was tested without the dust scheme implementation. The same situation happened to the dry deposition scheme proposed by Emerson et al. (2020) and Pleim et al. (2022). On the contrary, Kong et al. (2024) have updated the dust emission treatment in CMAQ applied for the East Asia region, but the response towards the new dry deposition schemes needs to be tested for future application. Due to the lack of observed deposition data in the western Pacific, adequate high-altitude (LABS) and ground observation data in Taiwan are essential references for verifying the model performance. With the advantage of high-altitude observation, LABS has detected the mixing aerosol type (dust and black carbon) that has not been widely explained, proving a good opportunity for model comparison. Under all of these research gaps, the model evaluation of multiple dry deposition schemes under the recently modified dust emission treatment, with the help of Taiwan's observation, can be vital. We have re-clarified the objective as follows:

"This study used the chemical transport model to investigate the long-range transport of East Asian dust (EAD) that occurred on 22-31 January 2023 and 12 March-20 April 2021. Due to the limitation of the dust model, the CMAQ version 5.4, embedded with three types of dry deposition schemes, was implemented to justify the effectiveness of improving our latest refined dust model (Kong et al., 2024). The dry deposition scheme proposed by Shu et al. (2022) has reduced certain model bias as compared to the base scheme. However, the revised scheme response to the natural phenomenon such as wind-blown dust has not being tested. In the other way, the number of concentrations of the large size particle has been decreased over land, and increased over ocean area globally by the adjusted collective coefficiency proposed by Emerson et al. (2020). Pleim et al. (2022) has included the consideration of white cap effect which dependent on wind speed and sea surface temperature into the dry deposition scheme. Hence, the response of the CMAQ dust model under the newly developed dry deposition schemes are worth investigating in reducing the model uncertainty.

LABS detected the recent transboundary episode in January 2023 as a mixing aerosol type (see Section 3.1), which has not been widely discussed, and the multiple dust storm episodes mentioned by Kong et al. (2024) provide an opportunity to model the EAD over the downwind region. Recognizing the significant transboundary events detected through Taiwan's observations, the improvement of the CMAQ dust model by the dry deposition schemes, and its application in characterizing the transport mechanism can be vital." **Page 4-5, line 97-115 in the revised manuscript.**

General comment 2: The abstract fails to mention the results presented in Figures 9–12 and they are only briefly emphasized in the final paragraph of the Summary and Conclusion section. Instead, the text focuses predominantly on comparisons between the dry deposition schemes and highlights E20 as superior.

Response: We thank the reviewer for the comment. The abstract and conclusion included more statement of Figures 10-12 (Figures 9-12 from the previous manuscript). To examine the dynamic between both aerosol types, we modified the surface resistivity at the smooth surface (R_b) from P22 to see how both aerosol types behave as responses to different R_b. Please see **General comment 5** for more detail.

The abstract has been revised. We modified as "… On 22-31 January 2023, the *in-situ* measurement of the upper level observed the possibility of natural dust and anthropogenic aerosol. This is consistent with the CMAQ, which shows that both aerosol types displayed a clear "long dust-black carbon belt" along the 15°N. It is revealed that the increase of wet deposition due to the surface resistivity (R_b) leads to a significant increase in dust mass concentration but a minor increase in black carbon (BC)...." **Page 1-2, line 28-32 in revised manuscript.**

The conclusion has been accordingly revised. We modified as "…It is worth revealing that the transboundary transport of EAD from the Asian continent towards the western Pacific Ocean at the upper level was associated with the eastward moving trough system. Such transport mechanisms have been found to bring along black carbon aerosol, which is primarily the main element of China's human-made emissions. More interestingly, both aerosol profiles created a "long dust-black carbon belt" along the 15°N. The 'double dome mechanism', a concept proposed by Huang et al. (2019) that depicts the superposition of the two aerosol types, was also simulated in the present study. Besides the similarity of both, the discrepancy in the case of the aerosol deposition and mass concentration was shown. By comparing the base P22 scheme to the revised scheme (P22E01-P22E03), wet deposition increases and hence increases the dust aerosol. In other ways, black carbon aerosol also increases in a minimal magnitude, not as much as dust aerosol. This study highlights the importance of dry deposition schemes for the modeled dust and black carbon concentration and provides a reference for better dry deposition schemes in CTMs over East Asia." **Page 18-19, line 488-499 in revised manuscript.**

General comment 3: Combined with the marginal statistical differences observed over a relatively short simulation period—despite the addition of 40-day simulations in 2021—this weakens the manuscript's scientific impact. In its current form, the paper is neither a comprehensive model comparison study nor a detailed test case analysis. It seems to attempt to address both objectives, but unfortunately, it falls short on both fronts.

Response: We thank the reviewer for the comment. We agree with the reviewer that a 10-day simulation might not be sufficient for the model comparison. However, due to the critical role of LABS in the western Pacific, the model comparison under the special long-range transport case is vital. To re-justify the impact of the dry deposition scheme on the CMAQ model, the 40-days simulation (multiple dust storm episodes) was used to double-check the results from the 10-days simulation. Overall, the simulated deposition velocity (V_d) during the 10-day simulation (January 2023) was consistent with the 40-day simulation (Spring 2021), as shown in Figure 7. The coarse mode of V_d under E20 during January 2023 and Spring 2021 was the lowest compared to S22 and P22. On the contrary, P22 recorded the highest V_d during both simulations. Such consistency of V_d during both periods leads to highest PM_{10} concentrations by E20, and lowest PM_{10} concentration by P22. The discussion on the simulated V_d (S22, E20 and P22) comparing the 40-day simulation in Spring 2021 and the 10-day simulation in January

2023, has been explained in detail. We modified it as follows: "Figure 7 shows the boxplot of the averaged simulated V_d for the Aitken, accumulation, and coarse particles modes under multiple deposition schemes in January 2023 (S22_2023, E20_2023, and P22_2023) and in Spring 2021 (S22_2021, E20_2021, and P22_2021). These different dry deposition treatments have a substantial impact on the aerosol profile, altering the ambient total dry deposition regionally. For instance, the median deposition velocity of S22_2023, E20_2023, and P22_2023 of the Aitken (accumulation) modes particle were 0.069 (0.020) cm s^{-1}, 0.039 (0.014) cm s^{-1} and 0.034 (0.029) cm s^{-1}, respectively. The E20 simulation median V_d decreased by -12.65 % for coarse-mode particles compared to S22. Also, the 75th percentile V_d of the coarse mode has been significantly reduced by -32.13 %. On the other hand, P22 showed a different simulation by the median V_d increment of 71.38 %. These findings suggest that the choice of dry deposition treatment can significantly influence the distribution and concentration of aerosols in the atmosphere, with potential implications for air quality and climate.

As shown in Figure 7, the results during the spring of 2021 are similar to those for the 2023 results for the median deposition velocity. For instance, the V_d Aitken, accumulation and coarse mode for E20_2023 (E20_2021) were 0.039 (0.039) cm s^{-1}, 0.014 (0.012) cm s^{-1} and 0.20 (0.19) cm s^{-1}, respectively. The result was consistent with the best simulated PM_{10} by E20 in 2023 and 2021 displayed in Table 3 and 4, respectively. The lowest V_d of the coarse mode particle was responsible for reducing the PM_{10} simulation underestimation of S22 and P22, consistent with the simulation by Ryu and Min (2022). The slow V_d means the total loss of aerosol to the surface has been minimized, leading to increased aerosol concentration. These implications are crucial for understanding the behaviour of aerosols in the atmosphere and their impact on air quality.

We estimated the CMAQ averaged particle modes for the S22_2023, E20_2023, and P22_2023 dry deposition scheme (Fig. 8). For S22_2023, we found that high V_d corresponding to the Aitken and accumulation modes distributed mainly over most of the CMAQ domain, which was most evident over Asian continent (Fig 8a, 8d). Meanwhile, the magnitude of V_d distribution was the most significant over the western Pacific Ocean by S22_2023 and the least for E20_2023 (dash rectangular box in Fig. 8d, e, f). For the coarse mode particles, the V_d was the lowest for E20_2023 compared to S22_2023 and P22_2023, particularly over the ocean area near northeast China, Japan, and Korea (white-dash rectangular box in Fig. 8d, e, f). This leads to a significant deposition over the downwind region, causing less PM_{10} simulated by P22_2023 and S22_2023 than E20_2023. A previous study proposed the V_d for the aerosol at the water surface was associated with the CTM uncertainly at the downwind region (Kong et al., 2021, 2024; Ryu and Min, 2022). The V_d at land surface was generally higher than at water surfaces. Interestingly, the coarse mode V_d at the water surface for E20_2023 (0.060 cm s^{-1}) was lower than S22_2023 (0.085 cm s^{-1}) and P22_2023 (0.116 cm s^{-1}), respectively, suggesting that E20_2023 deposition schemes could minimize the excessive deposition over the marine boundary layer (Table 5). Such minimal deposition velocity distributing over a large part of the western Pacific Ocean, including the Sea of Japan, Yellow Sea, East China Sea, and South China Sea, might be responsible for reducing the modeled PM_{10} underestimation over Taiwan (Fig. 8h), as mentioned by Kong et al. (2021).

To better understand the behavior of the V_d during the 40-day simulation of Spring 2021 corresponding to the aerosol simulation, we visualized the CMAQ averaged particle modes for the S22_2021, E20_2021, and P22_2021 dry deposition scheme (Fig. 9). The V_d of the coarse mode particles for E20_2021 was the lowest among the others over the ocean area, which shows similarity as E20_2023 (Fig. 9g, h, i). As mentioned by Kong et al. (2024), one

of the continuous EAD episodes was related to the typhoon. The strong wind speed and extreme precipitation due to the intense anticyclonic system caused nearly zero dust simulation. In S22_2021 (0.060 cm s^{-1}) and P22_2021 (0.070 cm s^{-1}), the model suggested high coarse mode V_d at the western Pacific Ocean. In E20_2021, the V_d (0.053 cm s^{-1}) is lower than the rest of the dry deposition mechanism, particularly the area affected by typhoon (black-dash rectangular box). This means that the E20 dry deposition has reduced the uncertainty of the excessive dust loss at the marine boundary layer. Figure 6 (g, h, i) shows more simulated mineral dust at the western Pacific by E20 than S22 and P22 during the spring of 2021." **Page 13-15, line 332-380 in revised manuscript.**

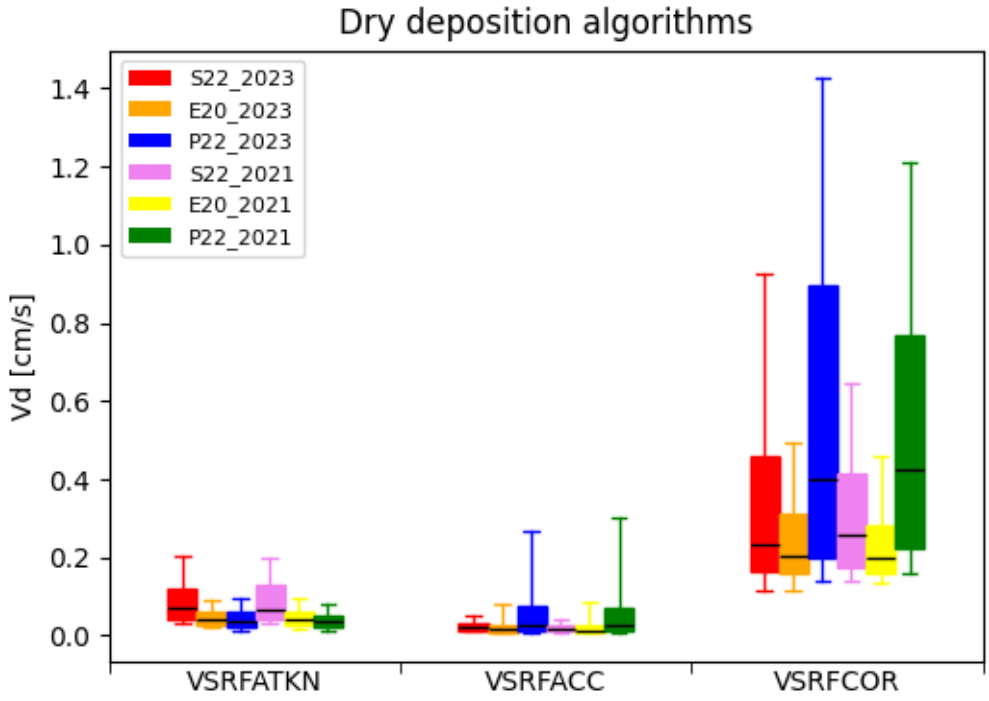

Figure 7: 10-days (2023) and 40-days (2021) averaged dry V_d predicted by CMAQ for the Aitken, accumulation, and coarse particle modes using the 2023_S22 (red), 2023_E20 (orange), 2023_P22 (blue), 2021_S22 (violet), 2021_E20 (yellow) and 2021_P22 (green) particle dry deposition schemes. The variability illustrated by the boxes and whiskers corresponds to spatial variability in annually averaged values throughout the CMAQ domain.

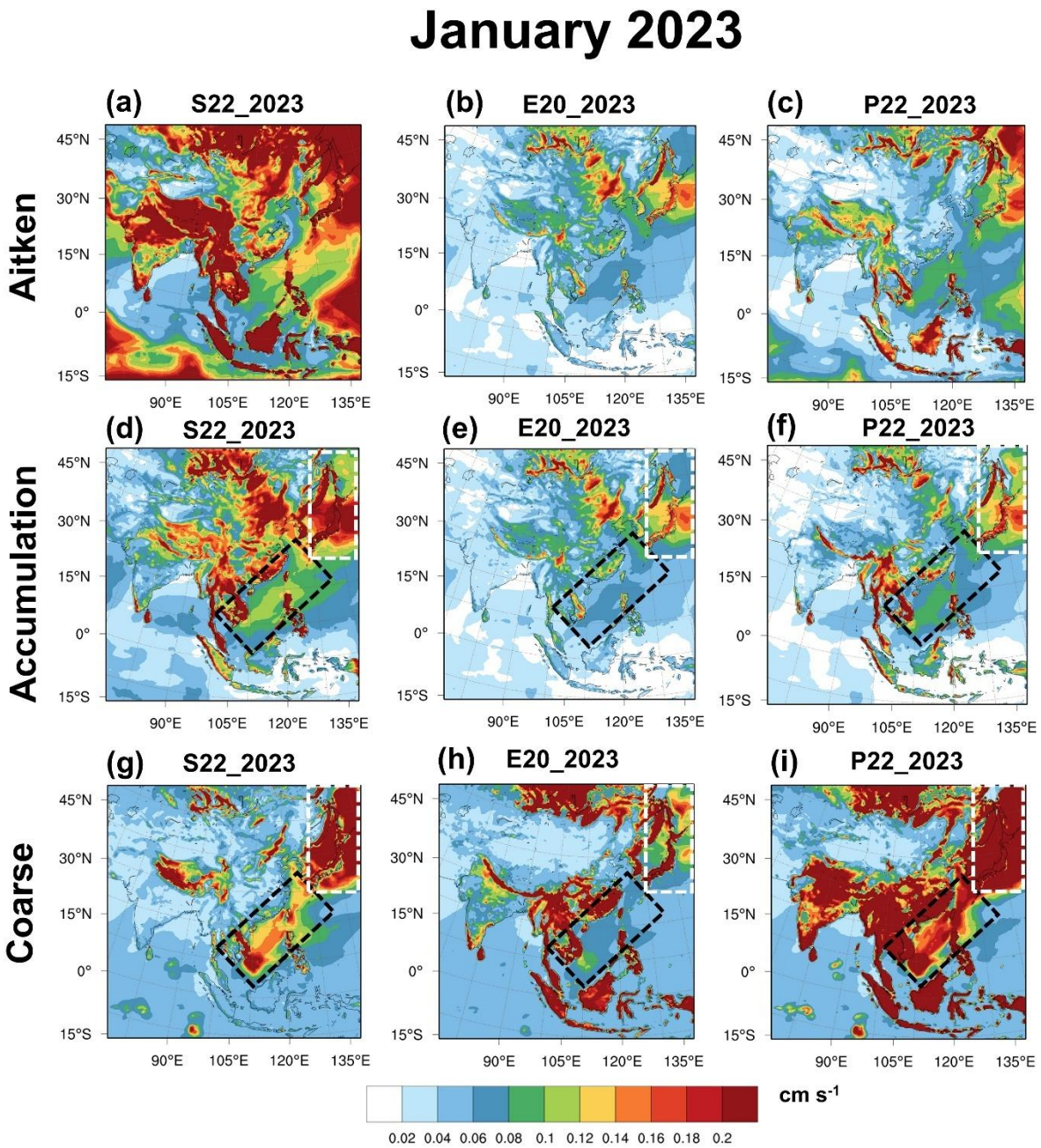

Figure 8: CMAQ estimated 10 days (22-31 January 2023) averaged for the (a-c) Aitken, (d-f) accumulation, and (g-i) coarse particle modes for (a, d, g) S22, (b, e, h) E20, and (c, f, i) P22 dry deposition schemes. White-dash rectangular indicates the region across northwest China; Black-dash rectangular indicates the marine boundary layer at the western Pacific.

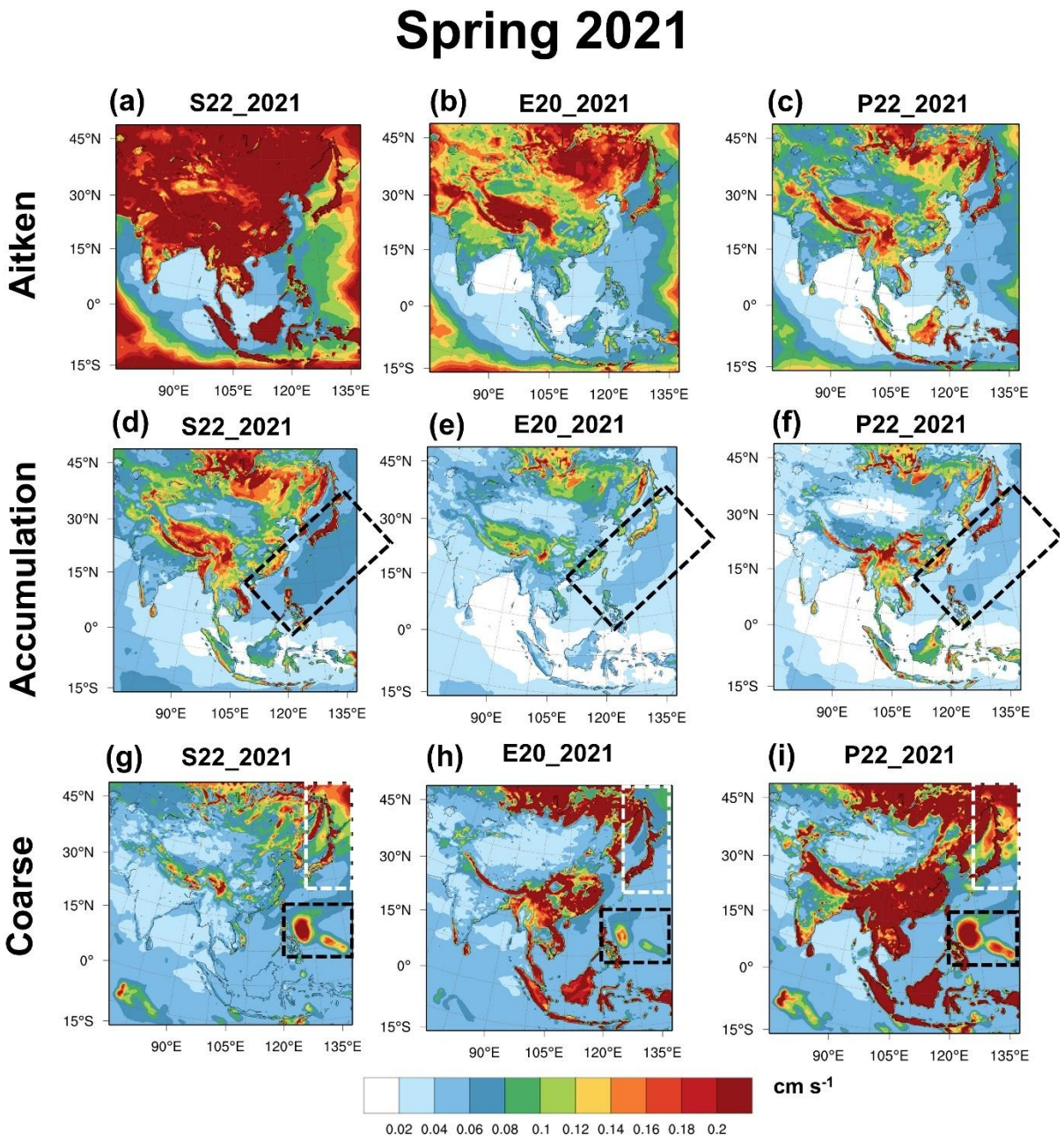

Figure 9: CMAQ estimated 40 days (12 Mar-20 April 2021) averaged for the (a-c) Aitken, (d-f) accumulation, and (g-i) coarse particle modes for (a, d, g) S22, (b, e, h) E20, and (c, f, i) P22 dry deposition schemes. White-dash rectangular indicates the region across northwest China; Black-dash rectangular indicates the marine boundary layer at the western Pacific.

General comment 4: Another major concern is the inconsistency between what is expected from the schemes based on their formulation and the existing literature versus what is reported in this manuscript. For example, P11 and P22 schemes are expected to be significantly different, as demonstrated in Figures 1–6 of Pleim et al. (2022). Yet, the authors report almost identical results for these models. They refer to the EPA analysis (https://github.com/USEPA/CMAQ/wiki/CMAQ-Release-Notes:-Dry-Deposition-Air-Surface-Exchange:-Surface-Tiled-Aerosol-and-Gaseous-Exchange-(STAGE)), which mentions only a 5% difference between the two schemes for CONUS. However, this analysis was not intended to compare P11 and P22 but rather to evaluate the implementation of P22 in M3Dry and STAGE. There appears to be confusion regarding the comparison of STAGE/M3Dry versus P11/P22. This can be clarified by noting that the "M3Dry" curve labeled in the EPA document (green curve) actually represents P22, not P11 (see Figures 2 or 3 of Pleim et al. (2022)).

Response: We thank the reviewer for the comment. The main difference between STAGE and M3DRY is the sub-grid scale variations in land use categories and the calculation of the component resistances. The present work's main objective is to compare different dry deposition schemes, namely S22, E20, and P22 on the CMAQ dust model. The present studies only focus on the STAGE dry deposition option to avoid confusion. The PR11(M3DRY) has been removed. We added the sentence as **"**Since the present study is primarily focused on the impact of dry deposition scheme on CMAQ dust model, the simulations with the STAGE module are the mandatory concern.**"** **Page 7, line 162-163 in revised manuscript.**

The result and discussion have been modified, particularly Section 3.2. We modify as:

"Table 3 shows the statistical analysis of PM_{10} and $PM_{2.5}$ concentrations over Cape Fuguei (northern Taiwan) from 22-31 January under the multiple deposition mechanisms. The threshold of the statistical index is based on Emery (2001). CMAQ_Off_S22, the PM_{10} simulation presented without the inline dust calculation, recorded the normalized mean bias (NMB) of -52.81 %. CMAQ_Dust_S22 improved the simulation over Cape Fuguei (northern Taiwan) by -47.01 % as we included the refined dust treatment (Kong et al., 2024). However, the improvement is insignificant due to the weak intensity dust episodes and the limitation due to the excessive deposition mechanism within the model (Kong et al., 2021). Hence, we expanded the sensitivity simulation to examine the impact of the deposition algorithm on the aerosol prediction. CMAQ_Dust_E20 simulations utilizing the Emerson et al. (2020) approach increased the modeled PM_{10} simulation by NMB of -41.9 %.

Instead of PM_{10} simulation, the present study found that the inline dust treatment and deposition algorithms could influence $PM_{2.5}$ simulation performances. For instance, the modeled $PM_{2.5}$ improved from -12.63 % (CMAQ_Off_S22) to -8.84 % (CMAQ_Dust_S22). Meanwhile, the deposition algorithm embedded in CMAQv5.4 has recorded modeled $PM_{2.5}$ by -10.65 % and -15.22 % under CMAQ_Dust_E20 and CMAQ_Dust_P22, respectively. This incident suggested that the East Asian dust from northwest China transported to the Western Pacific Ocean could also carry the anthropogenic emission of East China.

Figure 4 shows the time series of hourly PM_{10} and $PM_{2.5}$ concentrations over Cape Fuguei (northern Taiwan) and LABS (high altitude region) from 22-31 January 2023 under the multiple deposition mechanisms. Generally, all the patterns of PM_{10} simulations were consistent with the observed PM_{10}, especially in capturing the peak value. For instance, the maximum observed (CMAQ_Dust_E20) PM_{10} concentrations at the surface during Jan 24 and

27 were 141 (102.6) μg m^{-3} and 114 (163.2) μg m^{-3}, respectively. A similar time-series pattern was found for the $PM_{2.5}$ simulation (Fig. 4b).

More importantly, the CMAQ model performance over the high-altitude region needed to be carried out and discussed. The biomass-burning episode of the northern PSEA over Mt. Lulin has been finely correlated by plume rise injection (Chuang et al., 2016; Ooi et al., 2021). From Fig. 4c, the modeled PM_{10} pattern for CMAQ_Off_S22 could not correlate well with observed PM_{10} over Mt. Lulin, with a poor correlation of 0.30. The correlation was increased for CMAQ_Dust_S22 (0.54), CMAQ_Dust_P22 (0.46), and primarily well performed for CMAQ_Dust_E20 (0.55). The modeled result was somehow consistent with the surface PM_{10} simulation at Cape Fuguei. The high observed PM_{10} episodes during 27-28 January with a maximum of 34.5 μg m^{-3} was only 53.3 % higher than CMAQ_Dust_E20 of 22.5 μg m^{-3}. For the CMAQ $PM_{2.5}$, the simulation generally underestimated the observed $PM_{2.5}$.

During the spring of 2021, a series of dust storms (15 March, 27 March, and 18 April) occurred over the Gobi area, with one of the most significant dust storms in the past decade (15 March, the "3.15" dust storm hereafter) causing environmental impact over the continental (Jin et al., 2022; Gui et al., 2022; He et al., 2022; Liang et al., 2022; Tang et al., 2022). More interestingly, one of the multiple dust storm episodes reached western Pacific Ocean due to the extreme typhoon episode (Kong et al., 2024). Hence, we intend to re-emphasize the precision of various deposition schemes on the CMAQ for the recent dust storm episode over the Asian Continental highlighted by Kong et al. (2024). We evaluated the CMAQ simulations with the different dry deposition schemes for the 40-day sensitivity test on 12 March-20 April 2021 against measured PM_{10} and $PM_{2.5}$ concentrations across the observation sites in mainland China (Table 4). The observation sites used for the model comparison are marked in Fig. S1. Generally, the evaluation results for Taiwan and mainland China were consistent. During the 40 days of Spring 2021, the CMAQ PM_{10} of NMB was the highest for Off_S22 (NMB = -75.00 %), followed by Dust_S22 (-45.97 %). The latest inline dust emission scheme embedded with E20 dry deposition scheme for PM_{10} was well performed by NMB of -25.43 %, compared to the Dust_P22 (-59.82 %). For the $PM_{2.5}$ simulation, Dust_S22 has been improved from Off_S22, and Dust_S22 was slightly better than Dust_E20 and Dust_P22.

Figure 5 shows the scatter plot of simulated and observed PM across mainland China. The correlation coefficient (R), a factor of two (FAC2), and the mean observed and simulated PM are marked in Figure 5. The modeled PM_{10} without the dust scheme had the lowest correlation. Among all of these simulations, Dust_E20 performed the best correlation ($R > 0.3$) compared to Dust_S22 and Dust_P22. However, for $PM_{2.5}$, the correlation between the model and measured values was similar for all the dry deposition schemes. The statistical index of FAC2 was used in the present work since either low or high outliers less influence it (Chan and Hanna, 2004). The dataset is reliable for FAC2 values between 0.5 and 2.0, with the ideal model of 1.0. The simulated PM_{10} by Dust_E20 performed well, with a nearly perfect value of 1.1. Meanwhile, the $PM_{2.5}$ by Dust_S22 simulation was slightly better than Dust_E20 but much better than the other experiments.

The comparison of AOD between CMAQ and MODIS for the three dust storm episodes: 14-16 March 2021 ("3.15" dust storm), 26-28 March 2021 ("3.27" dust storm), and 17-19 April 2021 was shown ("4.18" dust storm) (Table 4). Overall, CMAQ Dust_E20 above 30°N has evaluated well the MODIS AOD by NMB of -26.2 %, as compared to S22 (-32.0 %) and P22 (-35.8 %). The CMAQ AOD by E20 during the most intense Super Dust Storm in 3.15 has significantly improved over northern China, the dust source region, as shown in the red

dash rectangular box (Fig. S3). Additionally, the modeled AOD by E20 over the western Pacific Ocean (shown in red dash rectangular box) increased in episode 4.18, reporting a value of 0.7 compared to 0.5 by S22. Significantly, the E20 deposition scheme has primarily enhanced the PM_{10} prediction over the marine boundary layer, addressing the model uncertainty due to the typhoon mentioned by Kong et al. (2024) and demonstrating the practical implications of our research.

The present work is consistent with the dust scheme in the WRF-Chem, where the dust loading is very sensitive to the dry deposition schemes and dust emission schemes, especially over the downwind region (Zeng et al., 2020). Fig. 6 shows the CMAQ estimated averaged mean PM_{10} and $PM_{2.5}$ in January 2023 and Spring 2021 for the Off_S22 and its corresponding change by Dust_S22, Dust_E20, and Dust_P22, respectively. Generally, the spatial distribution of the high PM_{10} concentrations by > 50 μg m^{-3} was distributed over northwest China, which is the dust source region's location, consistent with the simulation suggested by Kong et al. (2021, 2022, 2024). Such high particulate matter dissipated to east China, indicating the transport pathway in the southeastern direction towards the western Pacific (Fig. 6a, h). The larger PM_{10} distribution by E20 than S22 and P22 over northwest China, meaning E20 successfully increased the PM_{10} concentrations. Another fascinating fact about E20 was that the PM_{10} increased over the southern South China Sea (Fig. 6b). For the modeled $PM_{2.5}$ concentrations, the high concentration was distributed over the Asian Continental under all dry deposition mechanism." **Page 10-13, line 250-330 in revised manuscript.**

We modified Table 1, Table 3, Table 4, Table S1, Figure 4, Figure 5, Figure 6, and Figure S3 as:

Table 1. Model settings.

Model setting	Descriptions
Period	12 March-20 April 2021 and 22-31 January 2023
Domain	d01, d02, and d03 with 45 KM, 15 KM, and 5 KM of the resolutions, respectively
Boundary condition	NCEP FNL lateral boundary condition
Surface and land surface model	NOAH
Numerical weather model	WRF v40, including grid and observation nudging at d01.
Chemical transport model	CMAQ v5.4
Gas-phase chemistry and aerosol mechanism	CB06e51 + AE7
Emission Inventory	MICS-ASIA III emission in 2023, adjusted from the emission in 2017 (Zhang et al., 2018) based on the OMI-NO_x satellite (Huang et al., 2021).
Online dust treatment	The refined windblown dust treatment suggested by Kong et al. (2024).
Dry deposition option	STAGE (S22, E20 and P22).

Table 3. Statistical evaluation for PM_{10} and $PM_{2.5}$ concentrations during 22-31 January 2023 for Cape Fuguei under the multiple simulation scenarios.

	Benchmark	CMAQ						
		Off _ S22	Dust_ S22	Dust_ E20	Dust_ P22	Dust_ P22E01	Dust_ P22E02	Dust_ P22E03
		PM_{10}						
MeanObs		49.97	49.97	49.97	49.97	49.97	49.97	49.97
MeanMod		23.58	26.48	29.04	23.04	25.99	27.36	27.69
NMSE		0.66	0.56	0.49	0.71	0.57	0.53	0.52
NMB	± 85%	-52.81	-47.01	-41.90	-53.90	-47.99	-45.24	-44.58
R	> 0.35	0.43	0.46	0.52	0.42	0.48	0.51	0.52
NMBF		-1.12	-0.89	-0.72	-1.17	-0.92	-0.83	-0.80
		$PM_{2.5}$						
MeanObs		15.52	15.52	15.52	15.52	15.52	15.52	15.52
MeanMod		13.56	14.15	13.86	13.16	13.26	13.22	13.20
NMSE		0.30	0.30	0.29	0.31	0.30	0.30	0.30
NMB	± 85%	-12.63	-8.84	-10.65	-15.22	-14.54	-14.80	-14.92
R	> 0.35	0.50	0.53	0.53	0.52	0.53	0.53	0.53
NMBF		-0.14	-0.20	-0.12	-0.18	-0.17	-0.17	-0.18

Note: the definition of the statistical formulas NMSE: Normalized Mean Square Error; NMB: Normalized Mean Bias; R: Correlation Coefficient and NMBF: Normalized Mean Bias Factor

Table 4. CMAQ evaluation for PM_{10} and $PM_{2.5}$ against the averaged 100 observation sites across mainland China (Fig. S1) and AOD against MODIS daily observation near the dust source region (above 30°N) with Normalized Mean Bias (NMB) under the multiple simulation scenarios (Fig. S3). Spring 2021, 3.15, 3.27, and 4.18 represent the evaluation period by 12 March-20 April 2021, 14-16 March 2021, 26-28 March 2021, and 17-19 April 2021, respectively.

Parameters	Period	CMAQ						
		Off_ S22	Dust_ S22	Dust_ E20	Dust_ P22	Dust_ P22E01	Dust_ P22E02	Dust_ P22E03
PM_{10}	Spring 2021	-75.00	-45.97	-25.43	-59.82	-45.09	-35.42	-32.92
$PM_{2.5}$	Spring 2021	-55.56	-36.29	-37.50	-42.47	-41.20	-41.51	-41.66
AOD	3.15	-80.49	-46.41	-38.97	-48.45	-44.80	-41.66	-40.80
	3.27	-80.92	-41.84	-36.39	-44.52	-41.60	-39.30	-38.72
	4.18	-83.09	-7.83	-3.20	-14.52	-9.45	-7.18	-6.67
	Mean AOD	-81.50	-32.03	-26.19	-35.83	-31.95	-29.38	-28.73

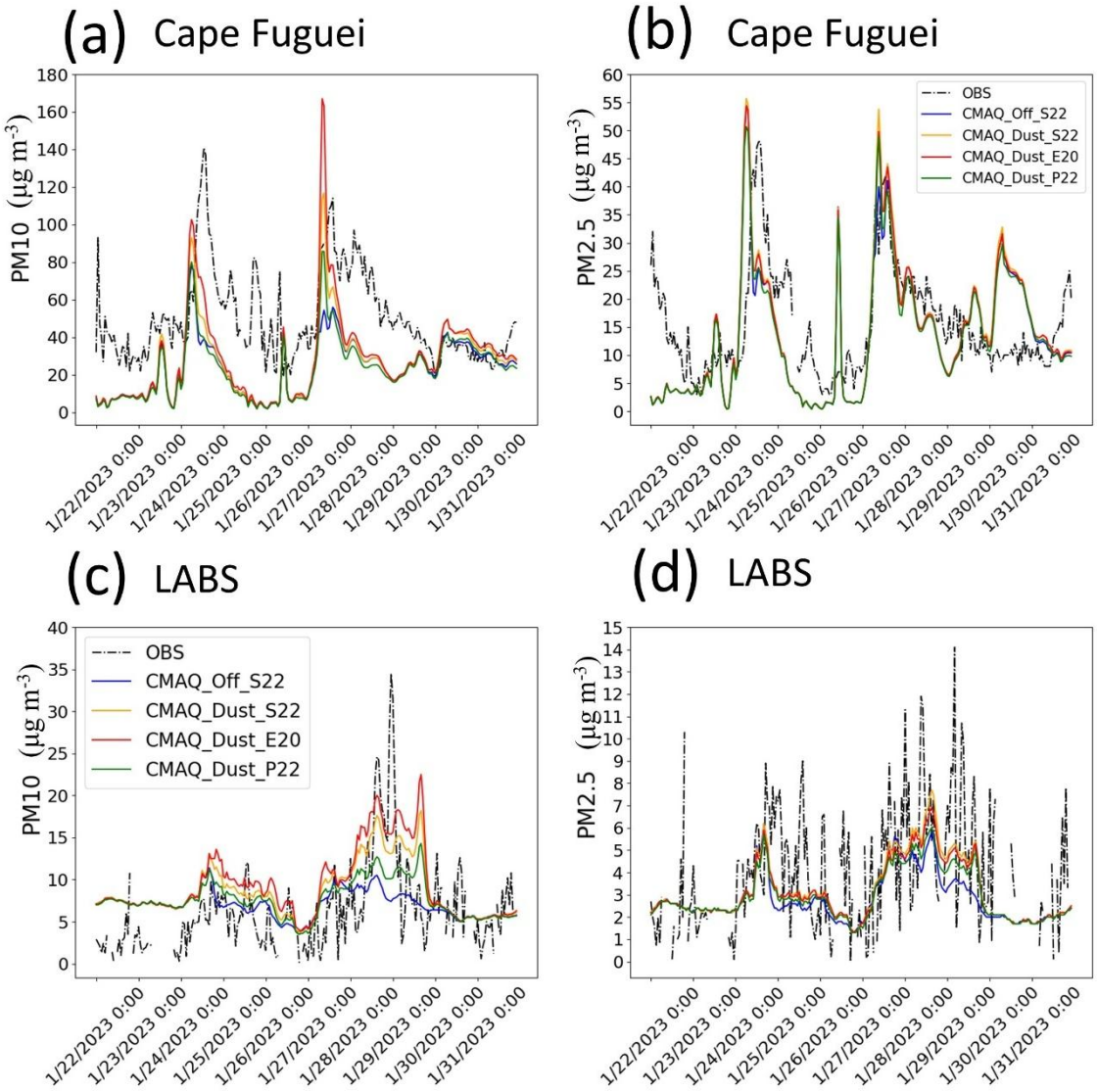

Figure 4: Time series of PM_{10} (left panel) and $PM_{2.5}$ (right panel) concentrations during 22-31 January 2023 under multiple deposition schemes over the Cape Fuguei (upper panel) and LABS (lower panel), representing the surface and high altitude, respectively.

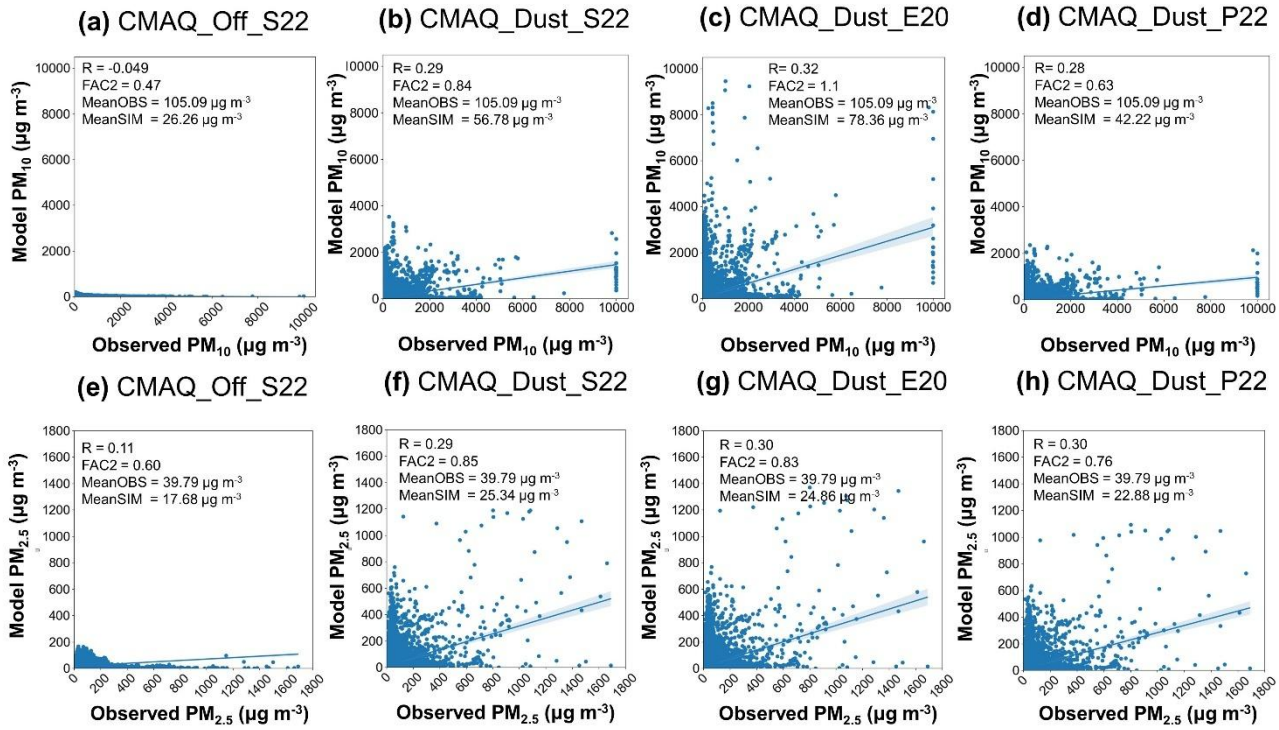

Figure 5: The scatter plot of the observed against modeled PM_{10} (a-d) and $PM_{2.5}$ (e-h) for CMAQ_Off_S22 (a, e), CMAQ_Dust_S22 (b, f), CMAQ_Dust_E20 (c, g) and CMAQ_Dust_P22 (d, h) at the 100 sites of the mainland China on 12 March-20 April 2021 (http://_). R is the correlation coefficient between the observation and model; FAC2 is the factor of two; MeanOBS and MeanSIM are the mean of PM from observation and model, respectively.

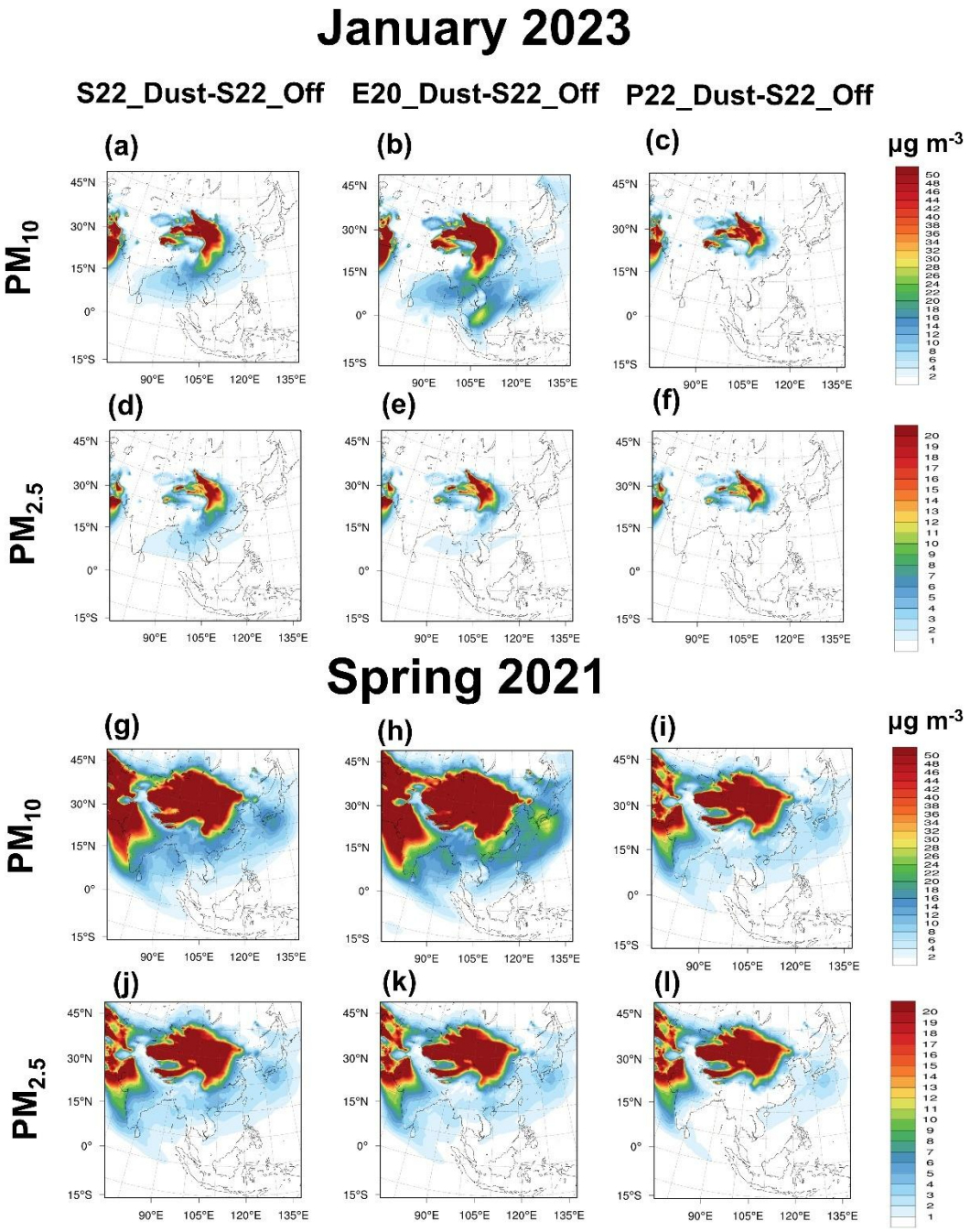

Figure 6: CMAQ estimated 10 days (January 2023) (a-f) and 40 days (Spring 2021) (g-l) averaged mean (a, b, c, g, h, i) PM_{10} and (d, e, f, j, k, l) $PM_{2.5}$ for the concentration changes using (a, d, g, j) S22, (b, e, h, k) E20 and (c, f, i, l) P22 schemes, as relative to the CMAQ_Off_S22 scenarios.

Table S1: V_d percentiles (cm s^{-1}) of atiken, accumulation and coarse particle modes by the three dry deposition schemes.

Dry deposition schemes	Percentiles	Aitken	Accumulation	Coarse
S22	25th	0.043	0.013	0.163
	50th	0.069	0.020	0.234
	75th	0.120	0.033	0.460
E20	25th	0.026	0.009	0.157
	50th	0.039	0.014	0.204
	75th	0.063	0.029	0.312
P22	25th	0.020	0.012	0.197
	50th	0.034	0.029	0.401
	75th	0.062	0.077	0.895

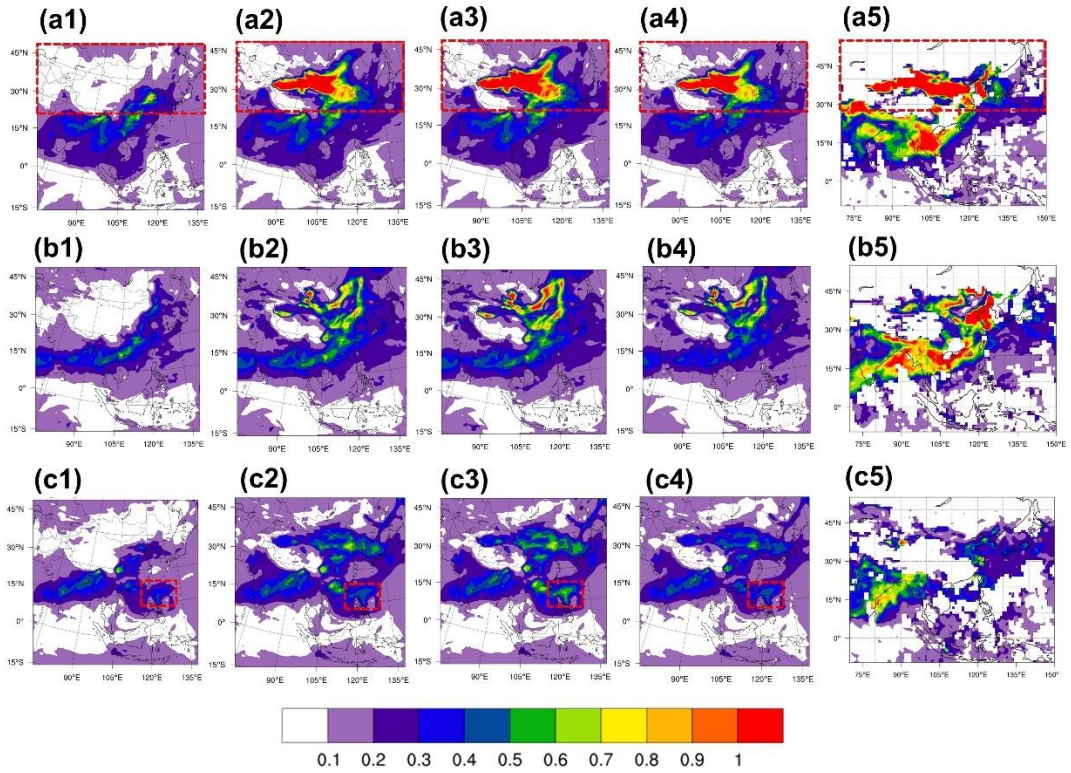

Figure S3: The 3-days mean averaged AOD over East Asia region, for (1-4) CMAQ and (6) MODIS during 14-16 March 2021 (a1-a5), 26-28 March 2021 (b1-b5) and 17-19 April 2021 (c1-c5). The simulations are the CMAQ_Off_S22 (a1, b1, c1), CMAQ_Dust_S22 (a2, b2, c2), CMAQ_Dust_E20 (a3, b3, c3) and CMAQ_Dust_P22 (a4, b4, c4).

General comment 5: If the goal is to conduct a true model comparison study, I recommend that the authors look deeper into the differences between the schemes and explicitly link their case study results to the schemes' formulations.

Response: We agree with the reviewer for the comment. The case study, schemes and its formulation were linked for explanation. As the case study in January 2023 is essential for the model evaluation over the western Pacific, the response of P22 on dust and black carbon has been carried out. This is because the P22 dry deposition scheme in CMAQv5.4 has included the white-cap effect over the ocean surface, which is related to the particle collection efficiency by impaction as a function of R_b at the smooth surface. Hence, the sensitivity of R_b by P22 should be tested for the western Pacific region like Taiwan, which is surrounded by the ocean. The R_b has been increased to a factor of 10, 50, and 100 under P22E01, P22E02, and P22E03, respectively. The dust aerosol can increase more significantly compared to black carbon with increased R_b. This means that the calibrating of R_b at the smooth surface can dramatically improve the dust model, potentially revolutionizing our understanding of the impact of the dry deposition scheme on the dust model. We revised the section as follows:

"Figure 10 illustrates mineral dust and BC concentration's spatial and temporal distribution under the CMAQ_Dust_E20 scenario at 700 hPa from 24-31 January. The model reveals a high proportion of modeled dust aerosol (red dash circle) at the source region, indicating an uplift from the surface to 700 hPa (Fig. 10a). This uplift, driven by the strong pressure gradient at the surface and the 'eastward moving trough system' at the upper level (700 hPa), is a key factor in the eastward and southward transfer of the dust (Fig. 10b). The high dust fraction reappears at the source region (Fig. 10c) and is transported eastwardly by the similar upper-level trough (Fig. 10d), causing a long dust belt at 15°N, distributing over central Asia continental, Taiwan Straits, Taiwan and large part of western Pacific Ocean. (Fig. 10e). On 29 January, the model of E20 clearly predicted that the dust plume moved in the southward direction toward the South China Sea (Fig. 10f). The dust aerosol was left distributed at a certain part of the northern South China Sea and the Philippine Sea until it totally dissipated (Fig. 10g, h). This interesting result suggests the possible EAD at the longer distance at the upper level, which is a topic for further investigation.

The southward high-pressure system responsible for the long-range transport haze episode has been widely discussed (Chuang et al., 2008; Kong et al., 2021)—however, the upper-level transboundary transport needs to be addressed more. While focusing on CMAQ_Dust_E20, we attempted to characterize the long-range transport of modeled black carbon at the upper level (700 hPa) (Fig. 10i-p). As shown in Fig. 10(i), the modeled black carbon concentration is shown to be significantly distributed at central China. The black carbon transport pattern followed the eastward-moving trough system as the plume moved eastward and southward (Fig. 10m, n). Interestingly, the long black carbon belt is consistent with the long dust belt, as shown in Fig. 10(e, f). For instance, both modeled dust and BC were distributed at the western Pacific Ocean (Fig. 10e, f, m, n) and South China Sea (Fig. 10g, o). This means that the BC due to the anthropogenic emission and the natural EAD shared a similar transport pattern at the upper level, driven by the trough system. Such consistency has been verified by the MERRA-2 dust and BC mass column over the region (red dash rectangular in Fig. S5).

The dust aerosol vertical profiles (Fig. 11) show a significant distribution of the large dust fraction over the Asian Continent under all simulation scenarios (Fig. 11a1-e1), as indicated by the transect drawn in Fig. 1. The westerly winds, depicted in Fig. 10, facilitated the eastward transport of the aerosol plume towards the western Pacific Ocean, where it

accumulated along the 700 hPa altitude. Another plume was observed across the ocean on the east side of Taiwan Island (Fig. 11b1). On 27 January, showed another substantial fraction of dust covering the Asian Continent and Western Pacific Ocean, with significantly higher dust concentrations compared to Fig. 11a1. The plume distributed eastward exhibited a clear dust dome (Fig. 11a5-e5). These findings have important implications for understanding and predicting dust aerosol transport patterns and their potential environmental impact.

The vertical profile of the modeled BC mirrors the transport pattern of mineral dust, as shown in Fig. 12. A transparent BC dome was distributed along 700 hPa, echoing the pattern observed for dust. This simulation suggests the consistency of the "double dome" mechanism of Asian dust and biomass burning episodes (Dong et al., 2018; Huang et al., 2019). The potential warming effect of such a mechanism is a topic ripe for future studies. However, it's important to note that the dust dome contains a higher fraction of concentrations than the black carbon dome. The present simulation suggests that dust aerosol can reach up to 500 hPa, which is consistent with Kong et al. (2021). On the other hand, the black carbon plume was slightly lower, with approximately 600 hPa of the maximum height under the same meteorological condition. This section, which discusses the similarity and distinctiveness of natural dust and anthropogenic aerosol at the upper level, highlights the need for further study. The present simulation did not consider the two-way coupling model, and it is strongly suggested for future research.

Table 6 shows the modeled deposition and mass concentration for different simulation scenarios in January 2023. The simulation of the wet deposition and mass concentration for dust aerosol was the highest by E20. This is consistent with the globally averaged aerosol number concentrations over the ocean for the large size particle (Emerson et al., 2020). Contrary, P22 was the lowest in simulated wet deposition and mass concentration. P22 could increase the accumulation mode's V_d and reduce the $PM_{2.5}$ over CONUS, which is similar to the present result (Pleim et al., 2022). Moreover, the present simulation by P22 showed the highest V_d of the coarse mode that leads to the less simulated PM_{10}. P22 revised the impaction collective efficiency, which is the parameterization of R_b. In order to understand the sensitivity of R_b on CMAQ simulation, the R_b has been scaled up, as shown in Table 2. Generally, the increment of R_b has gradually increased the wet deposition (surface mass concentration) by 13.6 (45.8) %, 25.2 (83.3) %, and 28.2 (93.7) %, under P22E01, P22E02 and P22E03, respectively. In addition, the increment intensity at the surface was higher than at the upper level. The simulated dust at western Pacific Ocean responding to the different dry deposition schemes was shown during 27 January in Figure 11 (red-dash rectangular box). As R_b increased by P22E01 and P22E03, the simulated PM_{10} by base scheme P22 (~30 μg m^{-3}), has increased to ~40 μg m^{-3} and ~50 μg m^{-3}, respectively. It is worth noted that P22E03 simulated a similar dust concentration as E20, indicating the importance of revising the R_b. On the contrary, the wet deposition and mass concentration were most significant for modeled BC under the S22 dry deposition scheme (Table 6). P22E01 only showed a minor increment, but it was nearly identical for P22E02 and P22E03 compared to P22." **Page 16-18, line 396-459 in revised manuscript.**

We modified Table 2, Table 6, Figure 11 and Figure 12 as:

Table 2. Simulation scenarios used in this present study.

Experiments	Online dust emission treatment by Kong et al. (2024)	Dry deposition treatment	Surface resistance (R_b) at the smooth surface
CMAQ_Off_S22	Off	S22	Default
CMAQ_Dust_S22	On	S22	Default
CMAQ_Dust_E20	On	E20	Default
CMAQ_Dust_P22	On	P22	Default
CMAQ_Dust_P22E01	On	P22	Increased by a factor of 10
CMAQ_Dust_P22E02	On	P22	Increased by a factor of 50
CMAQ_Dust_P22E03	On	P22	Increased by a factor of 100

Table 6. Model averaged dry, wet deposition and mass concentration for mineral dust and black carbon aerosols in January 2023 (10-days averaged) for different simulation scenarios.

Dust (ASOIL)	Dry deposition (mg m^{-2})	Wet deposition (mg m^{-2})	Mass concentration at the surface (μg m^{-3})	Mass concentration at 700 hPa (μg m^{-3})
S22	0.267	0.112	6.34	3.62
E20	0.167	0.136	10.25	4.40
P22	0.300	0.103	4.79	3.56
P22E01	0.243	0.117	7.00	3.79
P22E02	0.196	0.129	8.78	4.13
P22E03	0.183	0.132	9.28	4.22

BC (AECI + AECJ)	Dry deposition (μg m^{-2})	Wet deposition (μg m^{-2})	Mass concentration at the surface (ng m^{-3})	Mass concentration at 700 hPa (ng m^{-3})
S22	5.13	50.49	492	60.04
E20	8.09	48.27	471	57.73
P22	17.79	40.96	411	50.95
P22E01	16.88	41.64	415	51.23
P22E02	16.82	41.67	415	51.27
P22E03	16.82	41.67	415	51.27

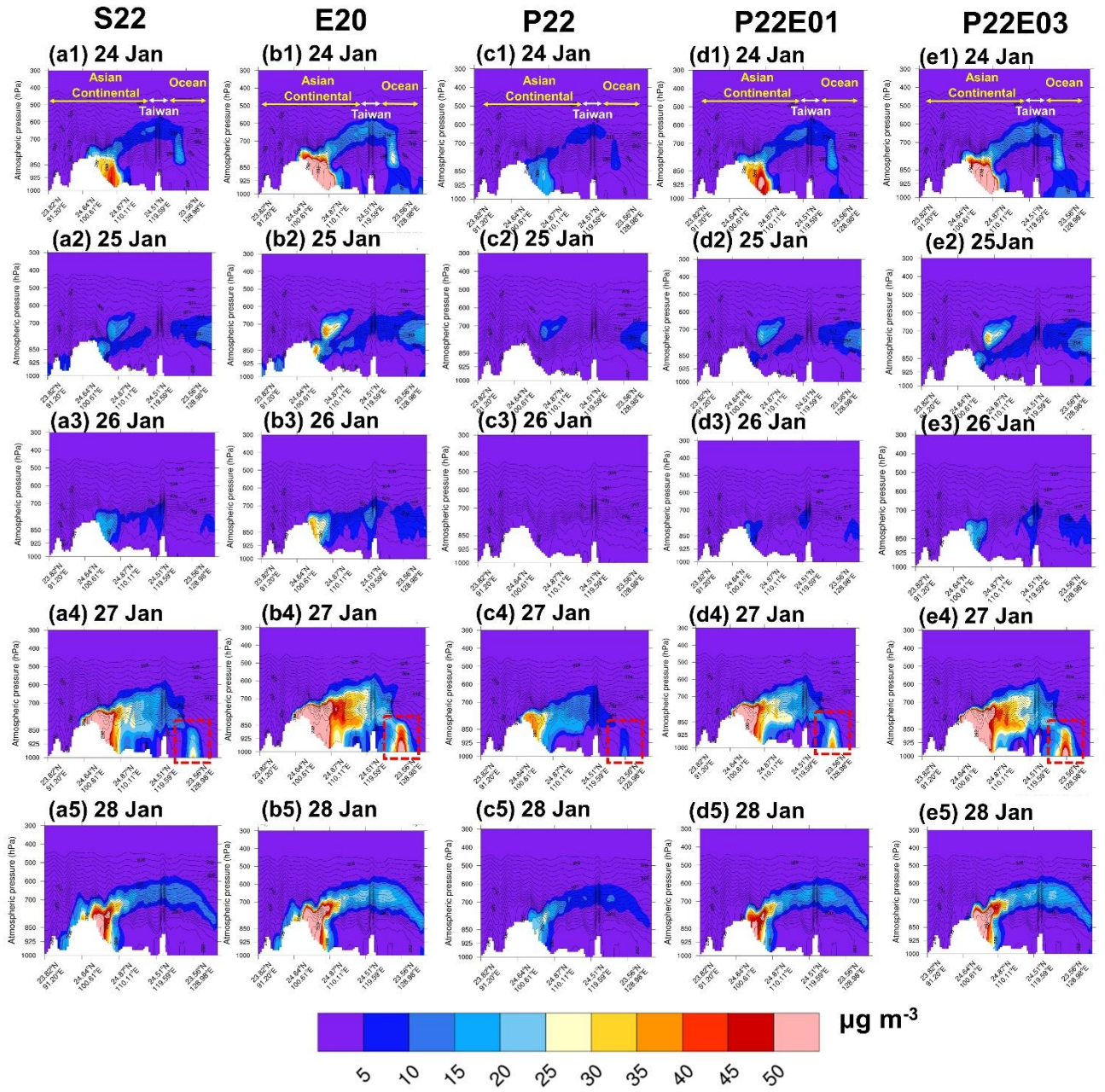

Figure 11: Vertical cross section of the simulated dust aerosol for the CMAQ_DUST (S22, E20, P22, P22E01 and P22E03) during 12 UTC 24-28 January 2023.

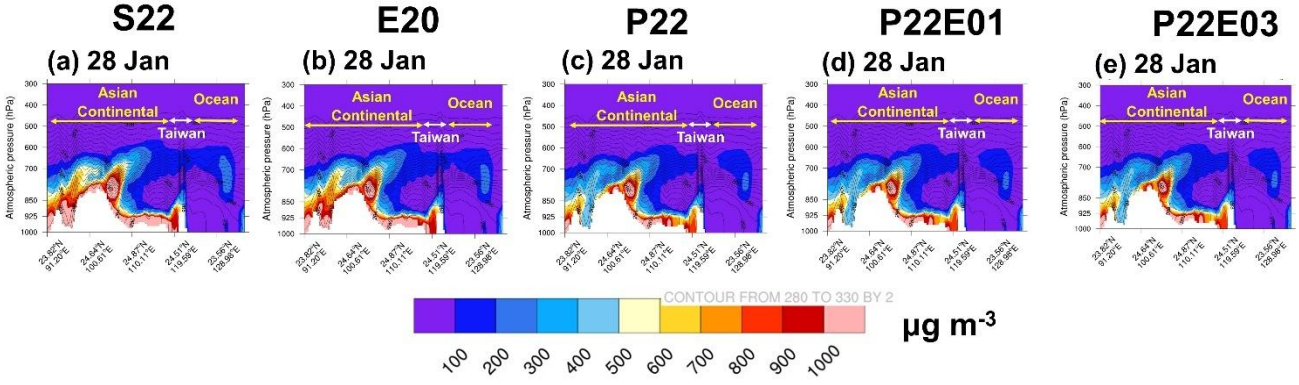

Figure 12: Vertical cross section of the simulated black carbon aerosol for the CMAQ_DUST (S22, E20, P22, P22E01 and P22E03) during 00 UTC 28 January 2023.